Independent control of mean and noise by convolution of gene expression distributions

Karl P. Gerhardt[1], Satyajit D. Rao[1], Evan J. Olson[1], Oleg A. Igoshin[1,2,3,4], Jeffrey J. Tabor[1,2]*.

[1]Department of Bioengineering, [2]Department of Biosciences, [3]Center for Theoretical Biophysics, [4]Department of Chemistry, Rice University, 6100 Main Street, Houston, Texas, 77005, USA

*Contact: jeff.tabor@rice.edu

Abstract

Gene expression noise can reduce cellular fitness or facilitate processes such as alternative metabolism, antibiotic resistance, and differentiation. Unfortunately, efforts to study the impacts of noise have been hampered by a scaling relationship between noise and expression level from a single promoter. Here, we use theory to demonstrate that mean and noise can be controlled independently by expressing two copies of a gene from separate inducible promoters in the same cell. We engineer low and high noise inducible promoters to validate this result in *Escherichia coli*, and develop a model that predicts the experimental distributions. Finally, we use our method to reveal that the response of a promoter to a repressor is less sensitive with higher repressor noise and explain this result using a law from probability theory. Our approach can be applied to investigate the effects

of noise on diverse biological pathways or program cellular heterogeneity for synthetic biology applications.

Introduction

Protein copy numbers vary within populations of genetically identical cells due to stochasticity in the molecular and cellular level events that impact gene expression[1–3]. This gene expression noise can be harmful, causing metabolic or physiological challenges, or reduce the reliability with which a cell can carry out a task[4–7]. Indeed, evolution appears to have optimized genomic locus[8], promoter architecture and sequence[9], transcription and translation rate[10], and selected for negative feedback[11,12] to decrease noise in the expression of toxic, complex forming, highly-connected, and essential proteins[8,10,13–16]. On the other hand, evolution has also exploited noise as a means to regulate stress response[17–19], alternative metabolism[20], cell-fate determination[21], and pathways enabling cell populations to divide labor or hedge bets against unpredictable environments[22,23].

Gene expression noise can be considered to contain an intrinsic component, relating to stochasticity in the chemical reactions of gene expression processes, and an extrinsic component, relating to noise in global conditions or upstream factors[1,24,25]. At low numbers of expressed proteins, intrinsic noise dominates and inversely correlates with the mean. At higher protein copy numbers, extrinsic noise becomes dominant and uncorrelated with the mean.

Tools that specifically modulate noise in the expression of genes of interest are needed to study the impact of noise on biological processes. However, controlling noise independently of mean is a major challenge due to the coupling between these two parameters[9,13,14,26–28].

Several strategies for decoupling mean and noise have been reported. For example, researchers have altered promoter activation kinetics[9,29,30], operator site location and multiplicity[31,32], and introduced transcriptional feedback[33–35]. However, multiple strains must be engineered to achieve different noise levels for the same mean using these methods. Independent control of mean and noise in a single strain requires manipulation of two separate processes impacting protein copy number[36]. This result has been demonstrated by combining two small-molecule responsive regulators in a cascade[37–40], altering both the frequency and bias of promoter state switching[41], tuning both transcription and mRNA degradation rates[42], or using a time-varying input to independently control promoter activation frequency and transcription rate[43].

One important limitation to all of these previous approaches is that they rely upon genetic parts, circuits, or pathways that are native to or have been optimized to function in a particular organism. As a result, substantial re-engineering may be required to achieve the same results in each new organism of interest. Additionally, there may be fundamental limitations on the levels of gene expression and noise that can be achieved using these approaches. For example, a two-step cascade primarily allows control of extrinsic noise as it relies on transmission of noise from the upstream regulator to the output[39,40].

Likewise, modulation of promoter kinetics is expected to primarily modulate intrinsic noise[39] and is unlikely to be effective at high copy numbers.

Here, we show that combining the protein expression distributions from multiple promoters in a single cell is a generalizable and straightforward strategy to achieve robust and independent control of mean and noise over a wide area. To this end, we first use a simple theoretical model to reveal that the mean and noise of a population distribution can be independently controlled using two co-expressed and orthogonally-regulated inducible promoters (IPs). We then implement this approach experimentally by constructing low and high noise generating IPs activated by the addition of two separate inducer molecules in *E. coli*. Next, we show that mean and noise of total gene expression can be manipulated using inducer combinations to control the activity of each IP. We characterize the steady-state behavior of cells harboring the IP pair and present a simple mathematical model to predict mean and noise from inducer concentrations. Next, we show that our experimental gene expression profiles can be predicted with high accuracy by simulating convolutions between the distributions contributed by each IP. Finally, we use our approach to independently tune mean and noise in the expression of a bacterial transcriptional repressor and analyze how each affects the activity of a target promoter independently.

Results

Model for independent control of mean and noise from two IPs

We considered two copies of a gene, encoding products G_1 and G_2, in a single cell. Here, the total amount of gene product, G, is $G_1 + G_2$. The mean (μ) value of G across a population of such cells is obtained from

$$\mu(G) = \mu(G_1) + \mu(G_2) \quad (1)$$

and the variance (σ^2) from

$$\sigma(G)^2 = \sigma(G_1)^2 + \sigma(G_2)^2 + 2Cov(G_1, G_2) \quad (2)$$

where Cov is the covariance. If G_1 and G_2 are regulated such that their expression is stochastically independent and the covariation negligible, the noise (η, defined as the standard deviation (σ) divided by the mean) of G is described by a weighted average of the noise from each source

$$\eta(G) = \left(\frac{\eta(G_1)^2\mu(G_1)^2 + \eta(G_2)^2\mu(G_2)^2}{(\mu(G_1) + \mu(G_2))^2}\right)^{\frac{1}{2}} \quad (3)$$

and the distribution of G in the cell population is described by a convolution

$$p_G(g) = \int_{-\infty}^{\infty} p_2(g - g_1)p_1(g_1)dg_1 \quad (4)$$

where p_1, p_2, and p_G are the probability density functions of G_1, G_2, and G, respectively. Conditions for stochastically independent G_1 and G_2 expression can be met if their dominant sources of noise are intrinsic or pathway specific[25].

Based on these results, we reasoned that mean and noise of G could be independently controlled by regulating G_1 and G_2 expression from low and high noise IPs (Fig. 1a). In this approach, $\eta(G)$ can be varied between $\eta(G_1)$ and $\eta(G_2)$ while maintaining constant $\mu(G)$ by tuning the relative expression of G_1 and G_2 with ratios of IP inputs (Fig. 1b). $\eta(G)$ can be tuned this way at different values of $\mu(G)$ by controlling the absolute expression of G_1 and G_2 with the amount of IP inputs. We also reasoned that the distribution of G can be predicted from a convolution of the distributions of G_1 and G_2 (Fig 1c). One attractive feature of this approach is the direct relationship between tunability and the difference in noise produced by G_1 and G_2. Therefore, IPs that produce large differences in noise over the same range of means are desirable when implementing this method.

Engineering a high noise promoter induced by AHL

To engineer a system capable of tuning noise over a wide range, we designed two IPs that produce similar mean expression levels with very different noise values. First, we engineered a high noise IP that incorporates positive autoregulation through the 3-oxo-C_6-acylhomoserine lactone (AHL)-dependent transcriptional activator LuxR and its target promoter P_{lux}. Specifically, we expressed a bicistronic mRNA encoding the reporter gene superfolder green fluorescent protein (*sfgfp*) and *luxR* as the output of P_{lux}. To achieve high noise levels and strong inducibility, we generated a small library of variants of this IP

with *luxR* ribosome binding sites (RBSs) of different strengths (Fig. 2a, Supplementary Fig. 1). Initially, we expected that stronger *luxR* RBSs would increase positive feedback strength by increasing the translational burst size of *luxR*. We believed that this effect would result in more *luxR* expression per AHL molecule, a steeper AHL-mean transfer function, and higher noise at intermediate IP outputs[44–46]. To examine the performance of these high noise IP designs, we separately transformed each construct into bacteria, treated the resulting strains with different AHL concentrations, and measured the resulting sfGFP fluorescence distributions via flow cytometry. To our surprise, weaker *luxR* RBSs result in increased steepness in the AHL-mean transfer function and higher noise in the AHL-noise and mean-noise transfer functions, respectively (Fig. 2b-d, Supplementary Fig. 1).

To understand these effects, we developed a deterministic kinetic model of the high noise IP family (Supplementary Methods, Supplementary Table 2). This model details the binding interaction between LuxR and AHL, as well as positive transcriptional autoregulation by LuxR:AHL. While such a deterministic model cannot predict gene expression noise, it allows us to analytically solve the steady-state response of the high noise IP family to AHL and identify design principles responsible for steepness of the transfer function. In particular, we find that this family of high noise IP designs is only sensitive to feedback when LuxR:AHL concentration is sensitive to LuxR fluctuations, i.e., when LuxR is limiting relative to AHL. At low *luxR* translation rates and intermediate AHL concentrations, the sfGFP output is bistable and exhibits hysteresis. Cell populations

undergo abrupt jumps from low to high states in this regime, resulting in steep AHL-mean transfer functions (Supplementary Fig. 2).

Within this bistable window, we expected noise-driven transitions between states to result in high gene expression variability. To verify this prediction, we constructed a stochastic kinetic model of the positive feedback circuit and computed AHL-mean and AHL-noise transfer functions using Gillespie SSA simulations (Supplementary Methods, Supplementary Tables 3 and 4). Mean and noise values quantitatively match experimental values for all four RBSs (Supplementary Fig. 3). For weak RBSs, noise reaches a maximum at intermediate AHL concentrations, while stronger RBSs show monotonic decreases in noise, further demonstrating ultrasensitive circuit transitions due to bistability.

Taken together, these kinetic modeling results capture the performance of our high noise IP family and recapitulate the unexpected inverse relationship between *luxR* RBS strength and the magnitude of feedback in the circuit. Among the high noise IP variants we tested, the variant containing the B0031 RBS generated the highest overall noise while maintaining unimodality. With this variant (hereafter named IP_h), we have constructed a high noise IP that satisfies our design criteria.

Engineering a low noise promoter induced by aTc

To produce low noise gene expression distributions over a wide range of mean values, we designed an IP wherein *sfgfp* is expressed under control of the Tetracycline Repressor

(TetR)-regulated $P_{Ltet-O1}$ promoter, with *tetR* expressed from a constitutive promoter on the same plasmid (Fig. 2e). We cloned the DNA encoding this IP into different plasmid backbones with ColE1 (50-70 copies/cell), p15a (20-30 copies/cell), and SC101* (3-4 copies/cell)[47] origins of replication (Fig. 2e). Initially, we hoped to find differences in output noise between origin of replication variants by virtue of the scaling between copy number and intrinsic noise, or by differences in plasmid copy number variability[25,47,48]. Mean output range (the difference between high and low states), detection threshold (inducer concentration at half output range), and steepness all increased with plasmid copy number (Fig. 2f, Supplementary Table 5). A deterministic kinetic model of the low noise IPs (Supplementary Table 6, Supplementary Methods) capture these experimental behaviors (Supplementary Fig. 4) and provides an explanation for why their transfer functions become steeper with increasing plasmid copy number.

For all origin of replication variants, we also observed that the sfGFP noise decreases monotonically as a function of both inducer and sfGFP mean until reaching a noise floor of about 0.25 (Fig 2g, h). At low induction, higher copy number variants produce lower noise but also correspondingly higher sfGFP mean, such that all variants collapse onto a similar initial trajectory. These behaviors suggest noise from this IP is dominated by intrinsic (at low to intermediate expression) and global extrinsic (at high expression) sources rather than transmitted noise from TetR or differences in copy number stringency between origins of replication. At intermediate induction, mean-noise transfer functions diverge slightly, with lower copy number variants decreasing more rapidly than higher copy number variants (Fig. 2h). A stochastic kinetic model of this low noise IP

(Supplementary Methods) recapitulates these experimental results, predicting monotonic decreases in noise as a function of aTc for all origin of replication variants, and lower noise at intermediate induction for lower copy number variants (Supplementary Fig. 3, Supplementary Tables 7-9).

These kinetic models recapitulate the behavior of our low noise IPs and reveal that the observed performance differences that arise on different plasmid backbones are attributable to differences in repressor and promoter copy number. The SC101* variant generates the lowest overall noise and similar sfGFP mean output levels as IP_h. Thus, we renamed this variant IP_l and carried it forward for further studies.

Independent control of mean and noise with low and high noise IPs

To demonstrate independent control of mean and noise by summing gene expression from low and high noise IPs, we co-transformed bacteria with plasmids encoding IP_h and IP_l (Fig. 3a). We exposed populations of the co-transformed bacteria to a 25 x 25 (625 total) panel of AHL and aTc concentrations and measured the sfGFP distributions by flow cytometry (Fig. 3b-d). We found that AHL-mean transfer functions are sigmoidal and shift higher with the level of aTc (Fig. 3b). This behavior is consistent with summation of sfGFP from IP_h and IP_l. Both the AHL-noise and mean-noise transfer functions decrease non-monotonically, peak at intermediate AHL concentrations, and shift lower with the level of aTc (Fig. 3c,d). These properties are consistent with noise being determined by the relative contribution of IP_l and IP_h to total sfGFP (Eq. 3). As intended, exposure to different inducer combinations produces an area in mean-noise space over which our system can

be tuned (Fig. 3d). Thus, we can independently control mean and noise by summing gene expression from low and high noise IPs.

As predicted by our model, a wide range of sfGFP noise values can be achieved at virtually the same mean (Fig. 3d-g). At low total bacterial fluorescence levels, differences between distributions with similar mean and disparate noise are masked by *E. coli* autofluorescence (Fig. 3f). However, as sfGFP levels increase and the contribution of autofluorescence to total cellular fluorescence becomes negligible, differences between distributions with similar mean and different noise levels become dramatic (Fig. 3e,f). Thus, while we can tune mean and noise at low and high expression levels, detecting tunability at low mean requires analysis after autofluorescence subtraction.

We next determined whether Eqs (1) and (3) could quantitatively recapitulate the behavior of this system. To that end, we adopted two phenomenological equations to describe mean and noise of each IP as a function of inducer, and fit their parameters to the experimental mean-noise data in Figure 3 (Supplementary Methods). Following this approach, we observe close agreement between model predictions and experimental data, enabling accurate prediction of mean and noise from inducer concentrations and further supporting the hypothesis of additive gene expression from our two IPs. (Fig. 3b-d, Supplementary Fig. 5, Supplementary Table 10).

IP_h/IP_l outperforms previous mean-noise control systems

To our knowledge, no metric has been proposed to describe the ability of a genetically-encoded system to independently tune gene expression mean and noise. The dynamic range, or ratio of output gene expression levels in the fully active versus fully inactive states, is a 1-dimensional metric frequently used to quantify IP performance. However, mean and noise are tunable over a 2-dimensional area[37–39,41–43].

To quantify the performance of mean-noise control systems, we developed metrics that we term dynamic area (F_A) and dynamic noise (F_η) (Methods). F_A measures the fold-change in mean-noise area over which a system can be tuned, while F_η measures the largest fold-change in noise a system can achieve at a constant mean. Practically, F_A describes the capacity of a system to produce different combinations of both mean and noise, while F_η captures the ability to modulate noise at a constant mean. We computed F_A and F_η using the experimental mean-noise dataset measured for our system and found values of 11.39 and 6.9, respectively (Fig. 3g). By this same analysis, we find that our system performs better than any previously described mean-noise control system (which range from 2.22 to 10.17 in F_A and 1.61 to 4.66 in F_η) we are aware of, in any organism (Supplementary Fig. 6, Supplementary Table 11).

Noise values among native *E. coli* genes range from 0.26 to 6.09 in a manner strongly dependent on the mean[13]. By comparison, our system can achieve noise values ranging from 0.318 to 2.18 at just a single mean (1045 MEFL, where F_η is defined), making our system capable of tuning noise through a range which is physiologically relevant to *E. coli*.

Convolution model predicts IP_h/IP_l distributions

We hypothesized that the distributions produced by our combined IP_h/IP_l system could be predicted by simulating a convolution between distributions generated by IP_l and IP_h individually (Fig. 4a). To examine this hypothesis, we simulated each of the 625 experimental populations resulting from exposure to the AHL and aTc panel in Figure 3 by summing randomly sampled fluorescence events between populations induced with only AHL and populations induced with only aTc (termed marginal distributions) (Fig. 4b, Methods). These simulated distributions show remarkable similarity to their experimental counterparts and frequently capture subtle, higher-order behaviors observed in experimental distributions such as skew and bimodality (Fig. 4b). While the simulated distributions are highly accurate overall, fluorescence levels are systematically overestimated in distributions with very low mean. This overestimation occurs because autofluorescence and basal sfGFP fluorescence (sfGFP fluorescence in the absence of inducer) are measured twice during the summation of two cell fluorescence events (Fig. 4a). Our distribution predictions are also less accurate when the AHL-induced population is near the inflection point of the AHL-mean transfer function (Fig. 3b).

We quantified similarity between each pair of experimental and predicted distributions using the Bhattacharyya coefficient[49] (c_B), a metric ranging from 0 to 1 measuring overlap between two probability distributions (Fig. 4b,c, Methods). The average c_B for all populations is remarkably high, at 0.92 with a standard deviation of 0.094. However, due to the previously-described effect of overestimating autofluorescence and basal sfGFP

expression, c_B shows strong correlation with expression mean below about 1,000 MEFL (Supplementary Fig. 7). Mean and standard deviation of simulated distributions show strong concordance with their experimental counterparts (ρ_c of 0.969 and 0.990 respectively) and this concordance is further improved (ρ_c of 0.995 and 0.993 respectively) after compensation for overestimated autofluorescence and basal expression (Fig. 4d,e, Methods). Overall, this approach of simulating convolutions between two experimental marginal distributions enables simple and accurate prediction of the total fluorescence distributions generated by our system.

Repressor noise decreases steepness of promoter response

The transcription factor-promoter transfer function is the quantitative relationship between transcription factor expression level and target promoter activity. It has previously been shown that the shape, including the steepness, of a transcription factor-promoter transfer function can strongly depend on the levels and context of transcription factor expression[50–54]. Based on previous experiments measuring the impact of noise on biological processes[29,37,43], we hypothesized that increasing noise in transcription factor expression would produce less steep transcription factor-promoter transfer functions. We used IP_h/IP_l to characterize the effect of repressor noise on mean expression from a target promoter. To that end, we first fused $PhlF^{AM}$ [50], a TetR family repressor from *Pseudomonas fluorescens*, to the C-terminus of sfGFP on both IP_h and IP_l. We then co-transformed *E. coli* with plasmids expressing the modified IP_h and IP_l along with an output plasmid carrying *mCherry* expressed under the $PhlF^{AM}$ repressed P_{PhlF} promoter (Fig. 5a). We grew these bacteria under different combinations of AHL and aTc, allowed sfGFP

and mCherry levels to reach steady-state, and quantified both fluorescent proteins by flow cytometry (Fig. 5b,c, Supplementary Figs. 8-10). As before, mean-noise transfer functions decrease non-monotonically with respect to AHL induction, peak at intermediate AHL concentrations, and shift lower upon addition of aTc (Fig. 5b). Conversely, induction with only aTc results in comparatively low noise, which monotonically decreases with higher mean (Fig. 5b). As a result, the system achieves different sfGFP-PhlF^{AM} noise while maintaining the same mean by applying different amounts and ratios of AHL and aTc. Mean mCherry fluorescence decreases in response to mean sfGFP-PhlF^{AM} in a manner that strongly depends on noise (Fig. 5c, Supplementary Fig. 10). When induced with AHL, mean mCherry begins to decrease at lower mean sfGFP-PhlF^{AM}, but requires dramatically higher mean sfGFP-PhlF^{AM} to become fully repressed compared to when induced with aTc (Fig. 5c, Supplementary Fig. 10). Moreover, induction with combinations of AHL and aTc generates intermediate levels of this effect. Noise, therefore, makes the PhlF-promoter transfer function overall less steep, increases apparent PhlF^{AM} activity at low mean, and decreases apparent PhlF^{AM} activity at high mean. This striking result demonstrates how a single transcription factor can generate vastly different population level behaviors depending on the details of its expression.

We applied a simple law from probability theory (Methods) to predict mean mCherry values from probability distributions of sfGFP-PhlF^{AM} (Supplementary Methods, Supplementary Fig. 11, Supplementary Table 12). While predicted mean mCherry values show a qualitative agreement with the data (Fig. 5d), strong cell autofluorescence signal

337 in the fluorescence distributions at low expression levels likely undermines a more
338 quantitative agreement.
339
340 **Discussion**
341 In nature, gene duplication has been proposed as a mechanism to resolve a tradeoff
342 between expression noise and environmental responsiveness[55]. This hypothesis was
343 recently validated for a pair of duplicated transcription factors in *S. cerevisiae*, where one
344 member of the pair exhibits low noise and is constitutively expressed, while the other
345 exhibits high noise and is induced by environmental stress[56]. This strategy appears to
346 have evolved to minimize transcription factor noise under normal growth conditions while
347 also allowing activation of a stress response pathway under stress-inducing conditions.
348 Based on the results of this study, we hypothesize that gene duplication may also allow
349 cells to adjust gene expression noise in order to increase fitness in environments where
350 low noise is beneficial and in other environments where high noise is beneficial.
351
352 Unlike previous approaches to modulating mean and noise in gene expression, our
353 method does not require the use of a particular genetic part or circuit, a specific
354 mechanism of noise reduction or amplification, or a particular host organism. Rather, it
355 only requires the availability of orthogonal low and high noise generating IPs in an
356 organism of interest and the ability to co-transform them into a single cell.
357
358 Though several mean-noise control systems have been reported, there had been no
359 method available to benchmark their performance against one another. Here, we propose

dynamic area and dynamic noise to quantify the performance of mean-noise control systems. These metrics capture the magnitude of the mean-noise area and the noise accessible at a constant mean, respectively. Like dynamic range, these metrics are independent of the absolute values of mean and noise. By comparing these two variables, one could distinguish systems that are tunable in both dimensions from systems that are primarily tunable in just a single dimension.

Our model based on summation of gene expression from two IPs accurately predicts population-level mean and noise of fluorescence distributions from inducer concentrations. The success of this approach supports the hypothesis for additive gene expression from our two engineered sources and may be adapted to describe future implementations of this method.

We can predict total gene expression distributions by simulating convolutions between experimental IP_l and IP_h distributions. While the predictions are systematically overestimated when autofluorescence and basal reporter gene fluorescence dominate (at low mean), they are otherwise surprisingly accurate and able to capture detailed population features that would not be predicted following a parametric approach. Going forward, our predictions would benefit from a method to reduce or deconvolve autofluorescence from flow cytometry measurements. While convolution predictions require advance measurement of marginal distributions, the number of convolutions that can be predicted combinatorially increases with number of marginal distributions measured. We imagine this predictive ability could be utilized to forward engineer desired

383 convolution distributions, including their higher moments and noise types, from existing
384 promoter libraries[57–63], constitutive or otherwise. Likewise, our method could be used to
385 combinatorially increase the number of gene expression distributions achievable with a
386 constitutive promoter library by expressing the same gene from combinations of two or
387 more library members.
388
389 Our results indicate that regulated promoters respond to their cognate transcription
390 factors at lower mean expression levels but require higher mean expression levels to
391 saturate as transcription factor noise increases. As a result, a noisy transcription factor
392 has higher apparent activity than a less noisy transcription factor at low expression levels,
393 while the opposite is true at high levels. These findings could be used to anticipate the
394 effect of changing the distribution of a transcriptional regulator or create design principles
395 for predicting and programming the shape of transcriptional dose-response curves.
396
397 Our method could be used to study other noise-dependent biological phenomena such
398 as transient stochastic resistance[19,64], persister cell formation[17,18], stochastic
399 differentiation[21], noise-induced cooperative behaviors[22,23], or gene circuit stability [65] in cell
400 populations. Such studies could provide a greater experimental basis for the fitness
401 advantages conferred by noise or be used to create design principles for engineering
402 desirable cell population behaviors using noise-driven processes.
403
404 Gene expression convolution could also be used to engineer noisy phenotypes into
405 populations of living cells. Example behaviors include genetically identical populations

406 that automatically differentiate into specified ratios of cell sub-types[66], form Turing-type
407 patterns using activator and inhibitor morphogens with similar diffusion rates[67], or
408 stochastically lyse in order to release enzymes to enable the population to metabolize
409 complex agricultural feedstocks[68]. Taken together, gene expression convolution is a
410 simple strategy for studying and controlling gene expression noise in a wide range of
411 organisms and biological pathways.
412
413 **Methods**
414 **Molecular biology**
415 The plasmids used in this study are listed in Supplementary Table 13**.** Plasmid maps are
416 shown in Supplementary Fig. 12. DNA assembly was performed by the Golden Gate
417 method[69], and cloning was performed in strain NEB 10β (New England Biolabs). A PhlF
418 mutant (PhlF^{AM}) with improved repression activity was amplified from the genome of strain
419 sAJM.1506[50] and used in this study.
420
421 **Cell growth and chemical induction**
422 *IP characterization and convolution experiments*
423 Experiments were performed in strain MG1655 in M9 media + 100 mM HEPES (pH 6.6)
424 at 37°C and 250 RPM of shaking. Media was supplemented with ampicillin (50 µg/mL),
425 spectinomycin (100 µg/mL), and chloramphenicol (35 µg/mL) as appropriate to maintain
426 plasmids.
427

Frozen preculture aliquots of each experimental strain were generated by growing transformants to exponential phase ($OD_{600} \approx 0.1$), adding glycerol to 18% (v/v), recording OD_{600}, and freezing 100 µL aliquots in PCR tubes at -80°C.

Panels of chemical inducer concentrations were prepared by diluting varying amounts of AHL (Sigma-Aldrich, K3007) in media, and aTc (Takara, 63130) in 100% ethanol, in wells of 96-well plates. Inducer concentrations in each panel well were prepared to 200X the desired final concentration. Panel plates were sealed with adhesive foil, stored at -30°C, and warmed to room temperature before experiments.

Experimental cultures were prepared by diluting a volume of preculture in media to achieve a cell density of $OD_{600} = 2 \times 10^{-5}$. Culture media was distributed among wells of 24-well plates (1 mL/well) and supplemented with the desired chemical inducer concentration by multichannel pipetting solution from chemical inducer panels. Culture plates were then sealed with adhesive foil and grown for 6 h to $OD_{600} \leq 0.3$, after which time they were iced for ≥ 15 min and measured by flow cytometry.

Transcription factor noise experiments

Experiments were performed as described above but in LB media. LB media was found to be necessary due to high metabolic burden from mCherry expression.

Flow cytometry

Flow Cytometry was performed with a BD FACScan flow cytometer outfitted with blue (488 nm, 30 mW) and yellow (561 nm, 50 mW) solid-state lasers (Cytek). sfGFP fluorescence was measured in the FL1 channel with a 510/20 nm emission filter, and mCherry fluorescence was measured in the FL3 channel with a 650 nm long-pass filter. Event rates of 1,000–3,500 events/s were used, and all events were captured until 20,000 events occurred within an SSC-FSC area characteristic of the strain. Calibration beads (Spherotech, RCP30-5A) were measured at the end of each cytometry session. Flow cytometry files were processed using FlowCal[70]. A gate fraction of 0.3 was used to gate events in the SSC and FSC channels, and FL1/FL3 arbitrary fluorescence units were calibrated to MEFL/MECY using calibration bead data collected during each respective cytometry session (Supplementary Fig. 13).

Population mean and variance calculation

Flow cytometry data for each sample was analyzed using a custom Python script that calculates arithmetic mean and noise from fluorescence distributions. The script first trims a small number of outlier observations which can heavily influence sample noise. Trimming is performed by first calculating a smooth estimation of the probability density function corresponding to the log-fluorescence distribution of the sample via kernel density estimation. The range of fluorescence values to keep is then determined by identifying the points nearest to the median at which the density estimate falls below a 0.5% threshold. Sample histograms that display the trimming effect are generated and assessed to ensure the trimming functions as expected. Mean and variance of a likewise

analyzed, untransformed MG1655 sample are then subtracted from the mean and variance of experimental samples.

System performance analysis

The concave hull of $\log_{10}$ transformed mean-noise pointsets was used to calculate both F_A and F_η. R packages "alphahull" and "sp" were used to find concave hulls and convert hulls to polygon objects, respectively. Alpha parameter was chosen manually. We report $\log_{10}(F_A)$ as the area of the polygon defined by the hull, and $\log_{10}(F_\eta)$ as the length of the longest vertical chord spanning the hull.

Convolution distribution simulation and analysis

Fluorescence events were randomly sampled (n=50,000) from populations that received no AHL and summed with likewise sampled events from populations that received no aTc. To simulate the population which received neither AHL nor aTc, events were sampled from that population twice and then summed. The three highest and lowest fluorescence events were eliminated before summation to remove extreme outliers.

Experimental and simulated fluorescence distributions were converted to density estimates, p_e and p_s, respectively, to calculate Bhattacharyya coefficients:

$$c_B = \int_0^\infty \sqrt{p_e(x_i)p_s(x_i)}dx \tag{5}$$

where x is FL1 fluorescence (MEFL).

Compensation of predicted mean and standard deviation was performed by subtracting the mean and variance of autofluorescence and basal sfGFP fluorescence from the uncompensated predicted mean and variance. Agreement between $\log_{10}$-scale experimental and simulated mean and standard deviation was measured by Lin's concordance correlation coefficient (ρ_c)[71].

Model for transcriptional output of a noisy regulator

Mean transcriptional output from the P_{PhlF} promoter was modeled using the Law of The Unconscious Statistician (LOTUS):

$$\mu(c) = \int_0^\infty f(x) p_e(x) dx \tag{6}$$

where mean mCherry expression, $\mu(c)$, of a population is found through a single-cell relationship, $f(x)$, between FL1 and FL3 fluorescence (Supplementary Methods) and the experimental FL1 probability density estimate $p_e(x)$. Model predictions in FL1 and FL3 were converted to sfGFP and mCherry by autofluorescence subtraction.

Statistical analysis

Points and density estimates throughout the text are single replicates collected over one to three separate experiments as indicated in figure legends. Standard errors on model fits are shown in the Supplementary Information.

Code availability

Custom code used in this study has been deposited on GitHub at https://github.com/taborlab/NoiseControl.

Data availability

Datasets generated during this study have been deposited on GitHub at https://github.com/taborlab/NoiseControl.

References

1. Swain, P. S., Elowitz, M. B. & Siggia, E. D. Intrinsic and extrinsic contributions to stochasticity in gene expression. *Proc. Natl. Acad. Sci. U.S.A.* **99**, 12795–12800 (2002).
2. Cai, L., Friedman, N. & Xie, X. S. Stochastic protein expression in individual cells at the single molecule level. *Nature* **440**, 358–362 (2006).
3. McAdams, H. H. & Shapiro, L. A bacterial cell-cycle regulatory network operating in time and space. *Science (New York, N.Y.)* **301**, 1874–7 (2003).
4. Schmiedel, J. M., Carey, L. B. & Lehner, B. Empirical mean-noise fitness landscapes reveal the fitness impact of gene expression noise. *Nature Communications* **10**, 3180 (2019).
5. Wang, Z. & Zhang, J. Impact of gene expression noise on organismal fitness and the efficacy of natural selection. *PNAS* **108**, E67–E76 (2011).
6. Duveau, F. *et al.* Fitness effects of altering gene expression noise in Saccharomyces cerevisiae. *eLife* **7**, e37272 (2018).

7. Keren, L. *et al.* Massively Parallel Interrogation of the Effects of Gene Expression Levels on Fitness. *Cell* **166**, 1282-1294.e18 (2016).
8. Batada, N. N. & Hurst, L. D. Evolution of chromosome organization driven by selection for reduced gene expression noise. *Nature Genetics* **39**, 945–949 (2007).
9. Raser, J. M. & O'Shea, E. K. Control of stochasticity in eukaryotic gene expression. *Science* **304**, 1811–1814 (2004).
10. Fraser, H. B., Hirsh, A. E., Giaever, G., Kumm, J. & Eisen, M. B. Noise Minimization in Eukaryotic Gene Expression. *PLoS Biol* **2**, (2004).
11. Ramsey, S. A. *et al.* Dual feedback loops in the GAL regulon suppress cellular heterogeneity in yeast. *Nat. Genet.* **38**, 1082–1087 (2006).
12. Ji, N. *et al.* Feedback control of gene expression variability in the Caenorhabditis elegans Wnt pathway. *Cell* **155**, 869–880 (2013).
13. Taniguchi, Y. *et al.* Quantifying E. coli Proteome and Transcriptome with Single-Molecule Sensitivity in Single Cells. *Science* **329**, 533–538 (2010).
14. Newman, J. R. S. *et al.* Single-cell proteomic analysis of S. cerevisiae reveals the architecture of biological noise. *Nature* **441**, 840–846 (2006).
15. Lehner, B. Selection to minimise noise in living systems and its implications for the evolution of gene expression. *Mol. Syst. Biol.* **4**, 170 (2008).
16. Barroso, G. V., Puzovic, N. & Dutheil, J. Y. The Evolution of Gene-Specific Transcriptional Noise Is Driven by Selection at the Pathway Level. *Genetics* **208**, 173–189 (2018).
17. Balaban, N. Q., Merrin, J., Chait, R., Kowalik, L. & Leibler, S. Bacterial persistence as a phenotypic switch. *Science* **305**, 1622–1625 (2004).

564 18. Rotem, E. *et al.* Regulation of phenotypic variability by a threshold-based
565 mechanism underlies bacterial persistence. *Proc. Natl. Acad. Sci. U.S.A.* **107**,
566 12541–12546 (2010).
567 19. El Meouche, I., Siu, Y. & Dunlop, M. J. Stochastic expression of a multiple antibiotic
568 resistance activator confers transient resistance in single cells. *Scientific Reports* **6**,
569 19538 (2016).
570 20. Carey, J. N. *et al.* Regulated Stochasticity in a Bacterial Signaling Network Permits
571 Tolerance to a Rapid Environmental Change. *Cell* **173**, 196-207.e14 (2018).
572 21. Balázsi, G., van Oudenaarden, A. & Collins, J. J. Cellular Decision-Making and
573 Biological Noise: From Microbes to Mammals. *Cell* **144**, 910–925 (2011).
574 22. Chen, L., Wang, R., Zhou, T. & Aihara, K. Noise-induced cooperative behavior in a
575 multicell system. *Bioinformatics* **21**, 2722–2729 (2005).
576 23. Ackermann, M. *et al.* Self-destructive cooperation mediated by phenotypic noise.
577 *Nature* **454**, 987–990 (2008).
578 24. Elowitz, M. B., Levine, A. J., Siggia, E. D. & Swain, P. S. Stochastic gene
579 expression in a single cell. *Science* **297**, 1183–1186 (2002).
580 25. Raser, J. M. & O'Shea, E. K. Noise in gene expression: origins, consequences, and
581 control. *Science* **309**, 2010–2013 (2005).
582 26. Bar-Even, A. *et al.* Noise in protein expression scales with natural protein
583 abundance. *Nature Genetics* **38**, 636–643 (2006).
584 27. Kim, K. H., Choi, K., Bartley, B. & Sauro, H. M. Controlling E. coli Gene Expression
585 Noise. *IEEE Trans Biomed Circuits Syst* **9**, 497–504 (2015).

586 28. Hornung, G. *et al.* Noise–mean relationship in mutated promoters. *Genome Res.* **22**,
587 2409–2417 (2012).
588 29. Blake, W. J. *et al.* Phenotypic consequences of promoter-mediated transcriptional
589 noise. *Mol. Cell* **24**, 853–865 (2006).
590 30. Murphy, K. F., Adams, R. M., Wang, X., Balázsi, G. & Collins, J. J. Tuning and
591 controlling gene expression noise in synthetic gene networks. *Nucleic Acids Res* **38**,
592 2712–2726 (2010).
593 31. Becskei, A., Kaufmann, B. B. & van Oudenaarden, A. Contributions of low molecule
594 number and chromosomal positioning to stochastic gene expression. *Nat. Genet.*
595 **37**, 937–944 (2005).
596 32. Murphy, K. F., Balázsi, G. & Collins, J. J. Combinatorial promoter design for
597 engineering noisy gene expression. *Proc Natl Acad Sci U S A* **104**, 12726–12731
598 (2007).
599 33. Becskei, A. & Serrano, L. Engineering stability in gene networks by autoregulation.
600 *Nature* **405**, 590–593 (2000).
601 34. Nevozhay, D., Adams, R. M., Murphy, K. F., Josic, K. & Balázsi, G. Negative
602 autoregulation linearizes the dose-response and suppresses the heterogeneity of
603 gene expression. *Proc. Natl. Acad. Sci. U.S.A.* **106**, 5123–5128 (2009).
604 35. To, T.-L. & Maheshri, N. Noise can induce bimodality in positive transcriptional
605 feedback loops without bistability. *Science* **327**, 1142–1145 (2010).
606 36. Briat, C. & Khammash, M. Computer control of gene expression: Robust setpoint
607 tracking of protein mean and variance using integral feedback. in *2012 IEEE 51st*

608 *IEEE Conference on Decision and Control (CDC)* 3582–3588 (2012).
609 doi:10.1109/CDC.2012.6426720.
610 37. Zhuravel, D. *et al.* Phenotypic impact of regulatory noise in cellular stress-response
611 pathways. *Syst Synth Biol* **4**, 105–116 (2010).
612 38. Blake, W. J., KAErn, M., Cantor, C. R. & Collins, J. J. Noise in eukaryotic gene
613 expression. *Nature* **422**, 633–637 (2003).
614 39. Aranda-Díaz, A., Mace, K., Zuleta, I., Harrigan, P. & El-Samad, H. Robust Synthetic
615 Circuits for Two-Dimensional Control of Gene Expression in Yeast. *ACS Synth Biol*
616 **6**, 545–554 (2017).
617 40. Bonny, A. R., Fonseca, J. P., Park, J. E. & El-Samad, H. Orthogonal control of mean
618 and variability of endogenous genes in a human cell line. *Nature Communications*
619 **12**, 292 (2021).
620 41. Hung, M. *et al.* Modulating the frequency and bias of stochastic switching to control
621 phenotypic variation. *Nature Communications* **5**, 4574 (2014).
622 42. Mundt, M., Anders, A., Murray, S. M. & Sourjik, V. A System for Gene Expression
623 Noise Control in Yeast. *ACS Synth. Biol.* **7**, 2618–2626 (2018).
624 43. Benzinger, D. & Khammash, M. Pulsatile inputs achieve tunable attenuation of gene
625 expression variability and graded multi-gene regulation. *Nat Commun* **9**, 3521
626 (2018).
627 44. Louis, M. & Becskei, A. Binary and graded responses in gene networks. *Sci. STKE*
628 **2002**, pe33 (2002).

629 45. Hooshangi, S., Thiberge, S. & Weiss, R. Ultrasensitivity and noise propagation in a
630 synthetic transcriptional cascade. *Proc. Natl. Acad. Sci. U.S.A.* **102**, 3581–3586
631 (2005).
632 46. Rossi, N. A. & Dunlop, M. J. Customized Regulation of Diverse Stress Response
633 Genes by the Multiple Antibiotic Resistance Activator MarA. *PLoS Comput. Biol.* **13**,
634 e1005310 (2017).
635 47. Lutz, R. & Bujard, H. Independent and tight regulation of transcriptional units in
636 Escherichia coli via the LacR/O, the TetR/O and AraC/I1-I2 regulatory elements.
637 *Nucleic Acids Res* **25**, 1203–1210 (1997).
638 48. Wong Ng, J., Chatenay, D., Robert, J. & Poirier, M. G. Plasmid copy number noise
639 in monoclonal populations of bacteria. *Phys. Rev. E* **81**, 011909 (2010).
640 49. Bhattacharyya, A. On a Measure of Divergence between Two Multinomial
641 Populations. *Sankhyā: The Indian Journal of Statistics (1933-1960)* **7**, 401–406
642 (1946).
643 50. Meyer, A. J., Segall-Shapiro, T. H., Glassey, E., Zhang, J. & Voigt, C. A. Escherichia
644 coli 'Marionette' strains with 12 highly optimized small-molecule sensors. *Nat.*
645 *Chem. Biol.* **15**, 196–204 (2019).
646 51. Schmidl, S. R., Sheth, R. U., Wu, A. & Tabor, J. J. Refactoring and optimization of
647 light-switchable Escherichia coli two-component systems. *ACS synthetic biology* **3**,
648 820–31 (2014).
649 52. Anderson, J. C., Voigt, C. A. & Arkin, A. P. Environmental signal integration by a
650 modular AND gate. *Mol Syst Biol* **3**, (2007).

651 53. Yokobayashi, Y., Weiss, R. & Arnold, F. H. Directed evolution of a genetic circuit.
652 *Proc. Natl. Acad. Sci. U.S.A.* **99**, 16587–16591 (2002).
653 54. Egbert, R. G. & Klavins, E. Fine-tuning gene networks using simple sequence
654 repeats. *PNAS* **109**, 16817–16822 (2012).
655 55. Lehner, B. Conflict between Noise and Plasticity in Yeast. *PLOS Genetics* **6**,
656 e1001185 (2010).
657 56. Chapal, M., Mintzer, S., Brodsky, S., Carmi, M. & Barkai, N. Resolving noise–control
658 conflict by gene duplication. *PLOS Biology* **17**, e3000289 (2019).
659 57. Mutalik, V. K. *et al.* Precise and reliable gene expression via standard transcription
660 and translation initiation elements. *Nat. Methods* **10**, 354–360 (2013).
661 58. Engler, C. *et al.* A Golden Gate Modular Cloning Toolbox for Plants. *ACS Synth.*
662 *Biol.* **3**, 839–843 (2014).
663 59. Fonseca, J. P. *et al.* A Toolkit for Rapid Modular Construction of Biological Circuits
664 in Mammalian Cells. *ACS Synth. Biol.* **8**, 2593–2606 (2019).
665 60. Lee, M. E., DeLoache, W. C., Cervantes, B. & Dueber, J. E. A Highly Characterized
666 Yeast Toolkit for Modular, Multipart Assembly. *ACS Synth. Biol.* **4**, 975–986 (2015).
667 61. Moore, S. J. *et al.* EcoFlex: A Multifunctional MoClo Kit for E. coli Synthetic Biology.
668 *ACS Synth. Biol.* **5**, 1059–1069 (2016).
669 62. Tschirhart, T. *et al.* Synthetic Biology Tools for the Fast-Growing Marine Bacterium
670 Vibrio natriegens. *ACS Synth. Biol.* **8**, 2069–2079 (2019).
671 63. Guiziou, S. *et al.* A part toolbox to tune genetic expression in Bacillus subtilis.
672 *Nucleic Acids Res* **44**, 7495–7508 (2016).

673 64. Meouche, I. E. & Dunlop, M. J. Heterogeneity in efflux pump expression predisposes
674 antibiotic-resistant cells to mutation. *Science* **362**, 686–690 (2018).
675 65. Turcotte, M., Garcia-Ojalvo, J. & Süel, G. M. A genetic timer through noise-induced
676 stabilization of an unstable state. *PNAS* **105**, 15732–15737 (2008).
677 66. Aronson, M. S., Ricci-Tam, C., Zhu, X. & Sgro, A. E. Exploiting noise to engineer
678 adaptability in synthetic multicellular systems. *Current Opinion in Biomedical*
679 *Engineering* **16**, 52–60 (2020).
680 67. Karig, D. *et al.* Stochastic Turing patterns in a synthetic bacterial population. *PNAS*
681 **115**, 6572–6577 (2018).
682 68. Egbert, R., Brettner, L., Zong, D. & Klavins, E. Self-destructive altruism in a
683 synthetic developmental program enables complex feedstock utilization. *bioRxiv*
684 086900 (2017) doi:10.1101/086900.
685 69. Engler, C., Kandzia, R. & Marillonnet, S. A one pot, one step, precision cloning
686 method with high throughput capability. *PloS one* **3**, e3647 (2008).
687 70. Castillo-Hair, S. M. *et al.* FlowCal: A user-friendly, open source software tool for
688 automatically converting flow cytometry data from arbitrary to calibrated units. *ACS*
689 *synthetic biology* (2016) doi:10.1021/acssynbio.5b00284.
690 71. Lin, L. I.-K. A Concordance Correlation Coefficient to Evaluate Reproducibility.
691 *Biometrics* **45**, 255–268 (1989).
692

693 **Acknowledgments**

694 We thank Dr. Joel Moake for the use of his flow cytometer. This material is based upon
695 work supported by the National Science Foundation under Grant No. CAREER 1553317

(PI: JJT), the Office of Naval Research under Grant No. N00014-18-1-2611 (PI: JJT), the Welch Foundation under Grant No. C-1856 (PI: JJT), the National Science Foundation under grant No. MCB-1616755 (PI: OAI), and the Welch Foundation under grant No. C-1995 (PI: OAI).

Author Contributions

K.P.G. and J.J.T. conceived of the project. J.J.T. and O.A.I. supervised the project. K.P.G. designed and constructed plasmids, performed experiments, and analyzed data. E.J.O. developed and wrote the code for calculation of sample mean and noise. S.D.R. developed and analyzed kinetic models of IPs. K.P.G. and E.J.O. developed the phenomenological model for IP mean and noise. K.P.G. developed and conducted performance analysis and convolution simulation technique. K.P.G., S.D.R., O.A.I., and J.J.T. wrote the manuscript.

Competing Financial Interests

The authors declare no competing financial interests.

Figures

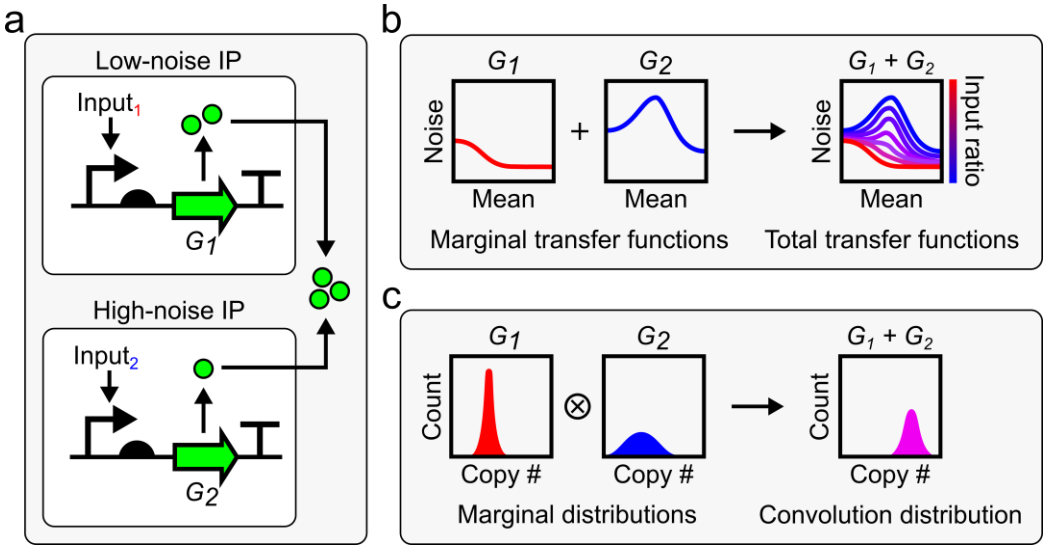

Fig. 1. Summation of gene expression from low and high noise IPs. (**a**) Two copies (G_1 and G_2) of the same gene are expressed from two independently regulated IPs: one that produces low noise distributions and one that produces high noise distributions. G_1 and G_2 sum inside cells. (**b**) Mean and noise of G_1 and G_2, separately, are functions of their respective IP's inputs (marginal transfer functions) and have single mean-noise trajectories. Mean and noise of the sum of G_1 and G_2 is a function of the amount and ratio of both IP's inputs (total transfer functions) and can be tuned within the area defined by their marginal transfer functions. (**c**) When G_1 and G_2 are summed, their marginal distributions form a convolution ($\otimes$).

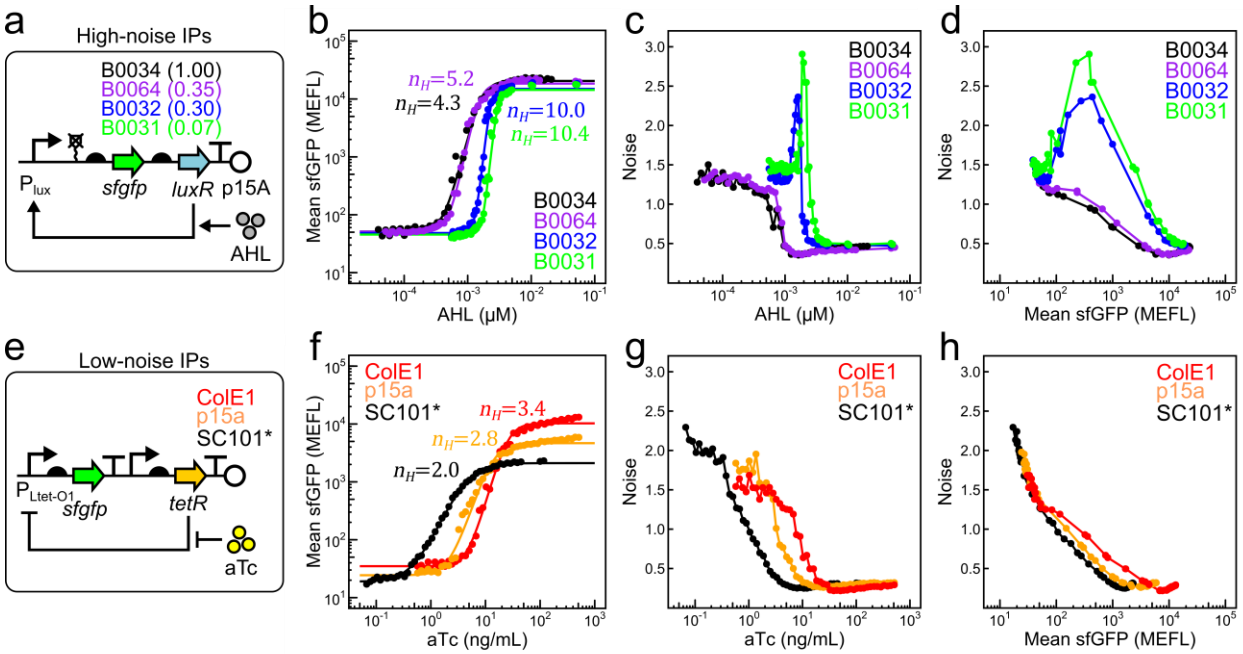

Fig. 2. Engineering low and high noise IPs controlled by AHL and aTc. (**a**) Library of high noise IPs based on LuxR:AHL-mediated positive transcriptional feedback. *LuxR* is encoded under RBSs of variable strength (indicated above the RBS) in different library members. Steady-state AHL-mean (**b**), AHL-noise (**c**), and mean-noise (**d**) transfer functions for high noise IP variants from (**a**). (**e**) Library of low noise IPs based on TetR:aTc-inducible gene expression without feedback. Different plasmid origins on which this IP is introduced are indicated. Steady-state aTc-mean (**f**), aTc-noise (**g**), and mean-noise (**h**) transfer functions for origin of replication variants from (**e**). Points within each group are single replicates collected from two separate experiments performed on two separate days. Smooth lines in (**b**) and (**f**) are fits to Hill functions with Hill coefficients (n_H) indicated.

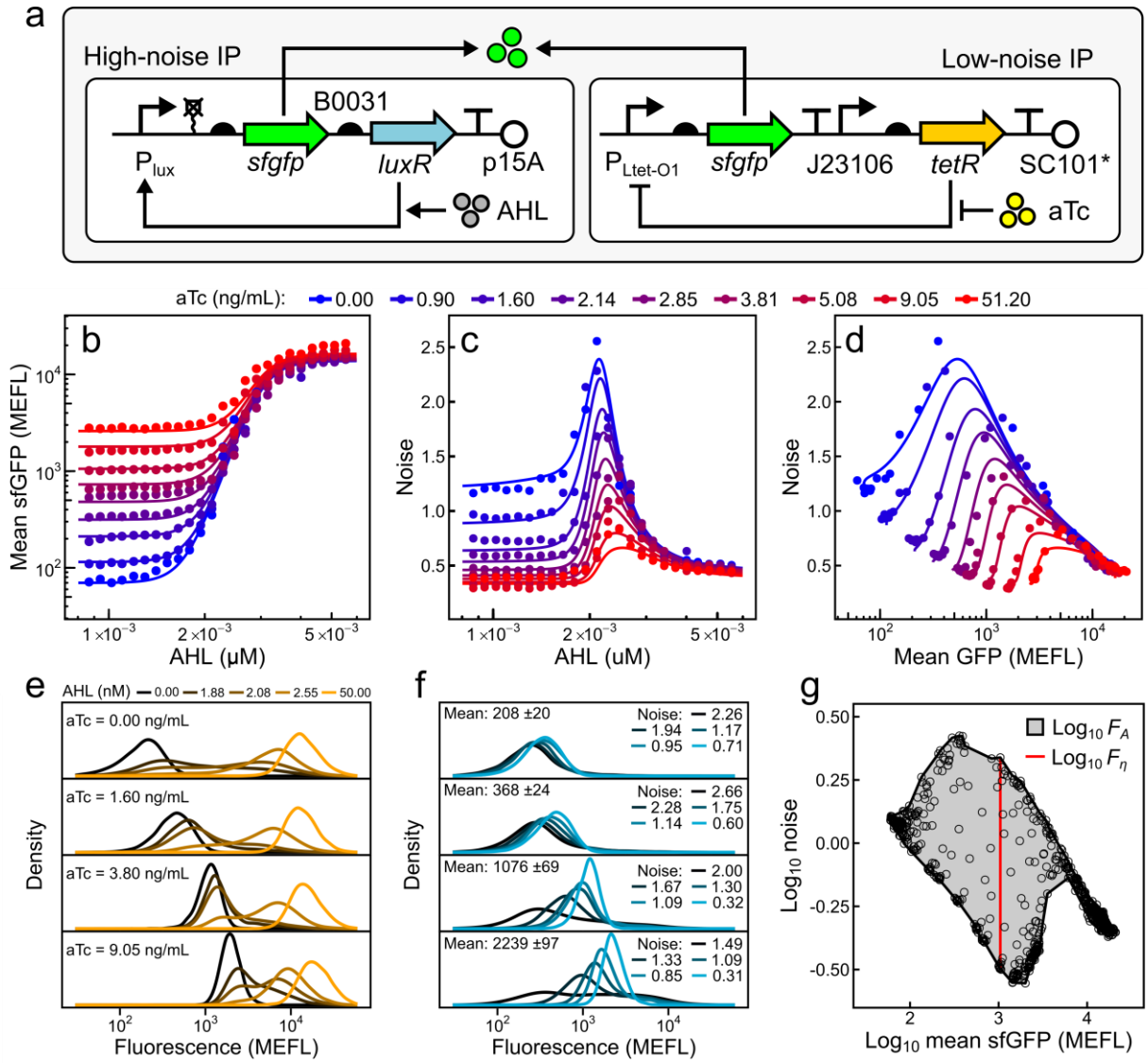

Fig. 3. Independent control of mean and noise by summation of gene expression from IP$_h$/IP$_l$. (**a**) Plasmids encoding IP$_h$ and IP$_l$ are co-transformed in MG1655 and induced with AHL and aTc, respectively. sfGFP from each IP sum inside cells. Steady-state AHL-mean (**b**), AHL-noise (**c**), and mean-noise (**d**) transfer functions of cells harboring plasmids in (**a**) with exposure to combinations of AHL and aTc. Mean and noise values (points) and model fits (lines) shown are a subset (9 out of 25 aTc concentrations) selected for evenly spaced visualization. Selected fluorescence density estimates of cell populations induced with AHL and aTc (**e**) over a wide range of inducer concentrations, or (**f**) to a wide range of noise at virtually the same mean. (**g**) Concave hull (black line) of the complete mean-noise pointset (circles) used to calculate dynamic area and dynamic noise. Points and density estimates are single replicates collected from three separate experiments performed on three separate days.

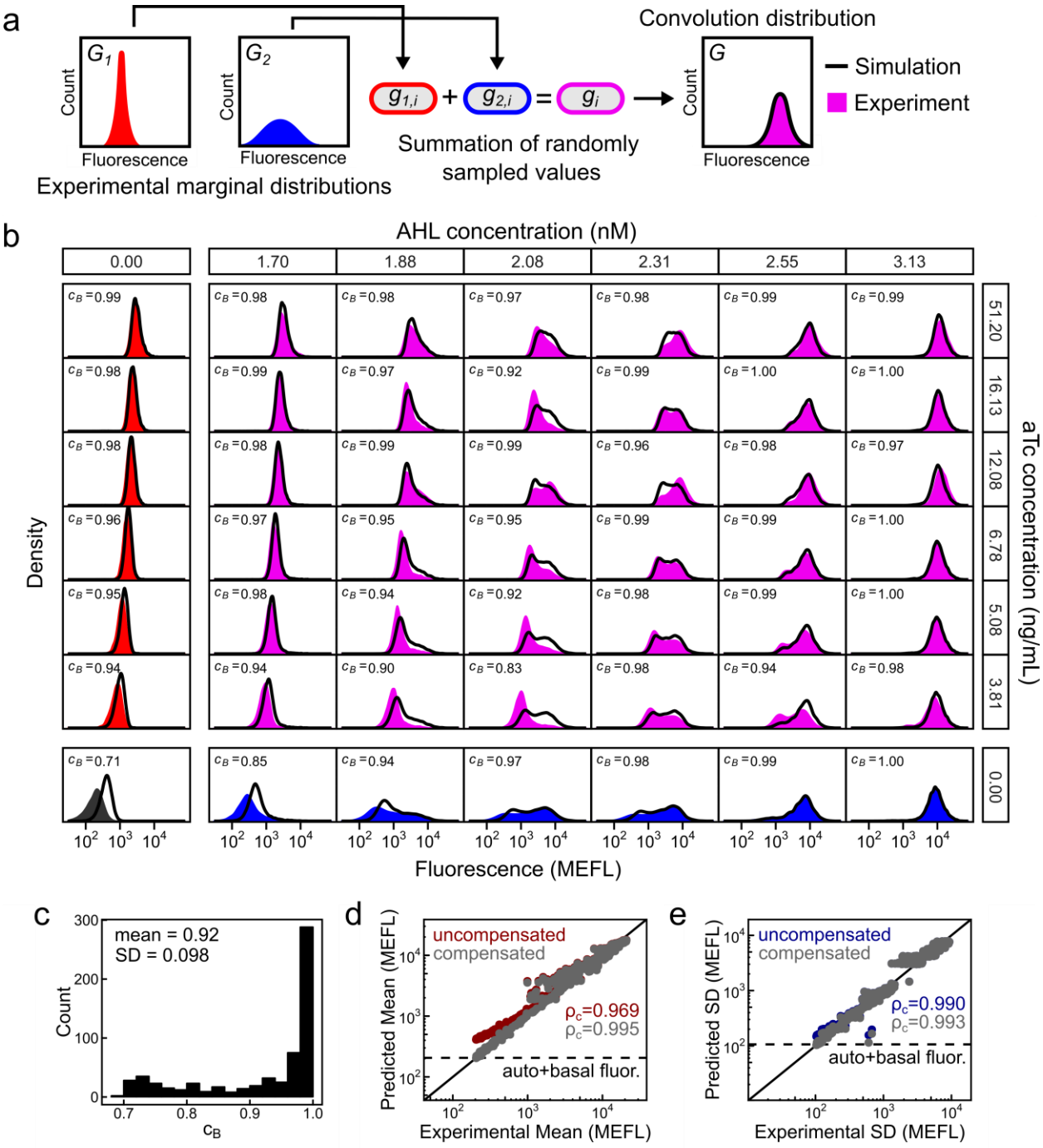

Fig. 4. Convolution predicts gene expression distributions from IP_h/IP_l. (**a**) Workflow for simulating convolution distributions. Fluorescence events from two experimental marginal distributions are randomly sampled and summed together. Summed events form a simulated convolution distribution which can be compared with an experimental counterpart. (**b**) Experimental (filled histograms) and simulated (black lines) fluorescence distributions of cell populations induced with combinations of AHL (vertically aligned, 7 of 25 shown) and aTc (horizontally aligned, 7 of 25 shown). Simulations were performed using populations with no AHL induction (first column) and no aTc induction (bottom row) as marginal distributions. Bhattacharyya coefficients (c_B) for each experimental-simulated

distribution pair is listed in each subpanel. (**c**) Distribution of c_B for all 625 pairs of experimental and simulated distributions. (**d**,**e**) Comparison of mean and standard deviation of experimental and simulated distributions. Equivalence line (black line) and Lin's concordance coefficients ρ_c are shown. Uncompensated predicted values measure autofluorescence and basal sfGFP fluorescence (dashed line) twice due to the summation in (**a**). Compensation is described in the **Methods**. Experimental density estimates are single replicates collected from three separate experiments performed on three separate days.

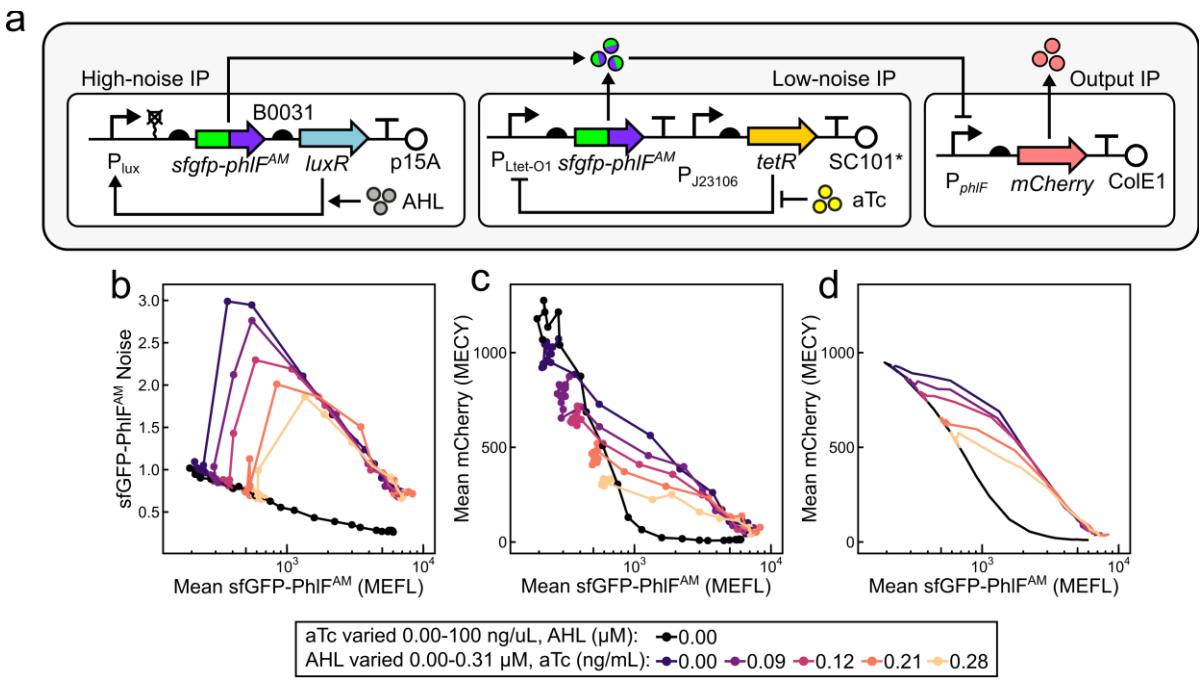

Fig. 5. Noise modulates repressor activity on a target promoter. (**a**) Schematic representation of plasmids used to control noise of a transcriptional regulator and monitor its output. PhlF^{AM} is fused to the C-terminus of sfGFP and expressed from IP_l and IP_h. PhlF^{AM} activity is monitored via mCherry expression from the P_{phlF} promoter on the output IP. (**b**) Steady-state sfGFP-PhlF^{AM} mean-noise transfer functions of cells harboring plasmids in (**a**) with exposure to combinations of AHL and aTc. (**c**) Mean mCherry expression as a function of mean sfGFP-PhlF^{AM}. (**d**) LOTUS model prediction of mean mCherry as a function of sfGFP-PhlF^{AM}. Points represent single replicates collected on a single day.